Dissimilar Electro-Osmotic Flow and Ionic Current Recirculation Patterns in Porous Media Detected by NMR Mapping Experiments

Bogdan Buhai and Rainer Kimmich

Sektion Kernresonanzspektroskopie, Universität Ulm, 89069 Ulm, Germany

(Received 1 August 2005; revised manuscript received 31 January 2006; published 2 May 2006)

Random-site percolation clusters were milled into ceramic (polar) and polystyrene (nonpolar) plates as a paradigm for porous media or complex microsystem channel networks. The pore space was filled with electrolyte solutions. Using NMR microscopy techniques, maps of the following quantities were recorded: (i) flow velocity driven by external pressure gradient, (ii) electro-osmotic flow (EOF) velocity, (iii) ionic current density in the presence of EOF, (iv) ionic current density in the absence of EOF. As far as possible, the experiments were supplemented by computational fluid dynamics simulations. It is shown that electro-osmotic flow as well as the electric current density include vortices and recirculation patterns. Remarkably, all transport patterns turned out to be dissimilar, and the occurrence and positions of vortices do not coincide in the different maps.

DOI: 10.1103/PhysRevLett.96.174501 PACS numbers: 47.56.+r, 76.60.Pc, 83.85.Fg

Electro-osmotic flow (EOF) arises when an electric field is applied to an electrolyte solution in channels with polar walls [1,2]. The wall surfaces become charged due to dissociation of polar groups of the wall material. The surface charges are compensated by surplus counterions in the solution. At thermal equilibrium, this net charge density decays from the highest value in the immobile ''compact layer'' directly at the surface down to zero across the mobile ''diffuse layer.'' In an electric field, the mobile surplus counterions in the diffuse layer are driven towards the coelectrode. That is, viscous friction between the surplus counterions and the solvent causes shear flow in the diffuse layer whereas the electrically neutral solution in the middle of the channel is characterized by a flat flow velocity profile.

This is the standard scenario one usually has in mind when speaking of EOF [3,4]. Corresponding NMR studies essentially revealing the ''plug flow'' characteristics of electro-osmotic velocity profiles have been published in Refs. [5,6]. However, when the electrolyte solution is filled into a complex channel network, totally different transport patterns arise particularly if the pore space is closed. In the present study, the unique capability of nuclear magnetic resonance (NMR) techniques to visualize and quantify velocity and electric current density (ECD) vector fields in complex geometries will be demonstrated. Velocity vector fields due to EOF and external pressure gradients are compared with electric current density vector fields in the presence and absence of EOF. Recirculation patterns and vortices are striking features of transport maps. In the comparisons following below, we will therefore focus on these characteristics.

The existence or absence of a similitude between fluid velocity and electric field is of crucial importance for microsystem devices as discussed in Ref. [7]. As a paradigm for complex systems, we have used a random-site percolation network [8] generated on a computer. The percolating cluster shown in Fig. 1 served both as a basis for computational fluid dynamics (CFD) simulations and as a template for the fabrication of real model objects. Identical pore spaces were milled on the one hand in glass ceramic plates (MACOR, Schröder Spezialglastechnik GmbH) as a polar material leading to EOF upon application of an electric potential gradient, and in polystyrene (PS) plates on the other. PS is nonpolar and, hence, does not show EOF. The fabrication technique is described in Refs. [9,10]. The in-plane size of the percolation object Fig. 1 is 100×100 pixels corresponding to 4 cm $\times$ 4 cm (or 6 cm $\times$ 6 cm if the inflow and outflow or electrode compartments are implied). The thickness of the pore space was 400 μm. Figure 1(b) shows a NMR spin density map [11] of water filled into the object. The computer generated template, Fig. 1(a), is obviously very well reproduced in the experiment. This demonstrates the reliability both of the fabrication and the NMR imaging methods.

For sensitivity reasons and in order to ensure the quasi-2D character required for the ECD experiments [12], 7–10 identical but independently fabricated model objects were stacked and studied at a time. Therefore, any potential imperfections such as surface defects are averaged out

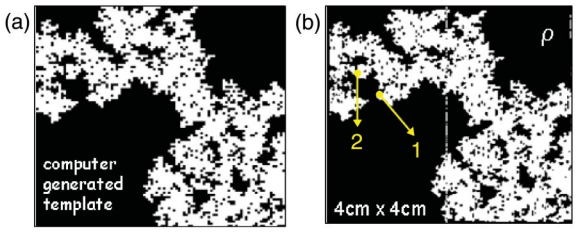

FIG. 1 (color). (a) Computer generated random-site percolation cluster (white). The porosity of the total percolation network (including isolated clusters not shown here) is $p = 0.6$. (b) NMR map of the spin density ρ of the water filled into to the pore space of an object fabricated on the basis of the template shown in (a). The matrix is again rendered in black. The areas marked by the numbers 1 and 2 refer to plots shown in Figs. 2 and 3.

and cannot be responsible for the observed transport patterns (compare Ref. [13]). The negligible influence of surface heterogeneities was also corroborated by test experiments with straight channels. The EOF eddies considered in Ref. [1], chap. 5, for this sort of device were not found in our experiments. The conclusion is that the pore space surfaces of our objects are homogeneous enough.

All experiments were carried out with a NMR tomograph consisting of a home made radio frequency console and a Bruker 4.7 T magnet with a 40 cm horizontal bore. The principles of flow velocity and electric current density mapping with NMR microscopy techniques are outlined in Refs. [11,12,14–16]. The echo time was 28 ms, the repetition time 4 s. The spatial resolution of the maps was in the range 180–270 μm. Velocities were resolved with an accuracy of 0.03 mm/s. The electric current density could be determined within $\pm 2\ \mu\mathrm{A/mm^2}$ [15]. The liquid state NMR signals on which the experimental maps are based solely originate from the water in the pore space.

For the EOF experiments, the object was filled with 1 mM $CaCl_2$ in distilled water. The conductivity of the bulk solution was 2.44×10^{-4} S/m. The gold electrodes consisted of two interdigitated combs in order to avoid eddy currents. The voltage applied across the 6 cm distance between the electrodes was in the range 300 to 900 V. The system was closed so that no inflow or outflow of the electrolyte solution was possible. The NMR velocity mapping pulse sequence is the same as described in Refs. [9,16] supplemented by a dc voltage applied during the whole echo time. The echo time was varied between 10 and 50 ms with no perceptible effect on the EOF velocity maps. Theoretically, one estimates a settling time of 28 ms according to Eq. (90) on p. 129 of Ref. [1]. Therefore, the assumption of steady state conditions is justified (compare Ref. [6]). Typical EOF velocity maps are shown in Figs. 2(a) and 3(b). The counterpart, pressure driven flow velocity maps are represented by Fig. 2(d). Detail maps for the area at position 1 [see Fig. 1(b)] are also shown in vector or streamline representation.

ECD mapping experiments were carried out again with an aqueous $CaCl_2$ solution, but with 10 times larger concentration and conductivity to optimize the ECD encoding efficiency (note that ECD mapping is based on a measuring principle totally different from velocity mapping). The pulse sequence is described in detail in Refs. [12,16]. The electric current pulses during the pulse sequence had a strength of 40 mA and were 4 ms long. The voltage across the objects (6 cm) was 300 V. The mean current density (magnitude) is estimated to be 36 $\mathrm{A/m^2}$. The precession phase maps recorded under the action of the current were ''unwrapped'' using Goldstein's two-dimensional unwrapping algorithm [17]. Typical ECD maps are shown in Figs. 2(b) and 3(c) recorded in the MACOR object, i.e., in the presence of EOF. This is to be compared with the ECD map, Fig. 2(c), measured in the PS object where EOF does not arise. Detail maps of the area around position 1 of Fig. 1(b) are again shown.

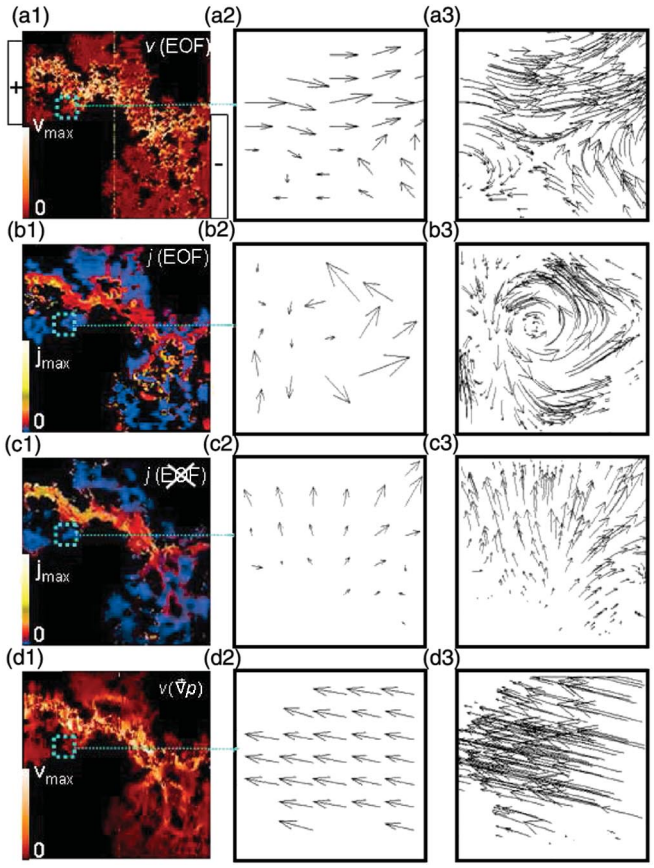

FIG. 2 (color). Left-hand column: Experimental maps of the magnitudes of different transport quantities measured in percolation model objects in a 4 cm $\times$ 4 cm field of view (see Fig. 1). The matrix is rendered in black. (a) EOF velocity, v(EOF), at a mean electric field strength of 83 V/cm (polar matrix). The position of the (closed) electrodes is indicated. (b) Electric current density in the presence of EOF, j(EOF) (polar matrix). (c) ECD in the absence of EOF, j (EOF off) (nonpolar matrix). (d) Flow velocity caused by an external pressure gradient in the open system, $v(\vec{\nabla}p)$. Middle column: Enlarged area at position 1 marked in Fig. 1(a) in vector plot form. The size is 1.2 mm $\times$ 1.2 mm. Right-hand column: Same as before, but now in streamline representation. That is, the vector arrows are bent along the local streamlines, and the length of the curvilinear vectors is proportional to the mean magnitude along the arrow. Typical maximum values for the velocity and electric current density are $v_{\max} = 4.5$ mm/s and $j_{\max} = 5\ \mathrm{mA/mm^2}$, respectively.

Hydrodynamic transport of an electrolyte solution in a polar porous medium is governed by pressure gradients, viscous friction, and electrostatic interaction between ions and external electric fields [18,19]. The flow velocity field, $\vec{v} = \vec{v}(\vec{r})$, is described by the Navier-Stokes equation assuming incompressible fluids and negligible gravitational forces. Under steady state conditions, this equation reads for external electrostatic forces

$$\rho_m(\vec{v}\cdot\vec{\nabla})\vec{v} + \vec{\nabla}p - \eta\nabla^2\vec{v} = \rho_q\vec{E}, \qquad (1)$$

where ρ_m and ρ_q are the mass and charge densities, respectively, η is the viscosity of the fluid, and $\vec{E}$ is the

electric field strength. The ''no-slip'' boundary conditions usually assumed at the pore walls ($v_{\text{wall}} = 0$) will, however, not be used for the CFD calculations (see below).

The electrostatic potential due to the electric double layer, Φ_{EDL}, obeys the Poisson equation

$$\nabla^2 \Phi_{\text{EDL}} = -\frac{1}{\epsilon_0 \epsilon} \rho_q, \tag{2}$$

where ϵ is the dielectric constant of the electrolyte solution, and ϵ_0 is the electric field constant. The charge density is distributed in the electrostatic potential according to a Boltzmann factor,

$$\rho_q = e \sum_i c_{i0} z_i \exp\left\{-\frac{z_i e \Phi_{\text{EDL}}}{k_B T}\right\}, \tag{3}$$

where e is the positive elementary charge, c_{i0} and z_i are the bulk concentration and the valence of the ith ionic species, respectively, k_B is Boltzmann's constant, and T is the absolute temperature. The boundary condition for the Poisson equation in the Debye-Hückel approximation is given by the ζ potential on the surface and is zero at infinity [1].

A finite element CFD method [20,21] was employed for comparison with the experiments. Since the electric double layer at the pore walls is not resolved in the experiments by far, there is no need to do so in the simulations. That is, instead of a no-slip boundary condition at the surfaces, an effective slip boundary condition is used. The numerical solutions were obtained with the aid of the software package FEMLAB 3 [22]. The model assumed in the calculations is described in Refs. [22,23]. The simulations were performed using a network of triangular meshes with 65 268 elements and 453 443 degrees of freedom for the two-dimensional percolation cluster used as a template for the model object. Any effects of chemical reactions between the walls, electrodes and solution were neglected.

Figure 4 shows a comparison of simulated EOF streamlines and vector plots for open [Fig. 4(a) and 4(b)] and closed electrodes [Fig. 4(c) and 4(d)]. ''Open'' means that there are infinite electrolyte solution reservoirs at both electrodes permitting unrestricted inflow and outflow. The streamline patterns simulated in two dimensions turned out to be similar to experimental velocity maps although the quasi-2D model objects in reality are 3D, of course. The third dimension, in particular, means that the friction and electroosmosis at the planes covering the pore space at the top and at the bottom should be considered. Corresponding simulations require, however, excessive computer capacity which was not available. Comparisons of experimental maps with two-dimensional simulations in this study or those in Ref. [7] can therefore be only of a qualitative nature. The simulations reveal the same phenomena as the experiments and therefore rule out any eddy current artifacts by field gradient pulses employed during the pulse sequences [12]. The influence of Taylor-Aris dispersion effects on EOF [24] can be excluded on the same basis.

EOF is strongly modified by hydrodynamic pressure gradients built up in the pore system. Flow in pore spaces sealed at the electrodes are characterized by a tendency to form recirculation patterns and vortices. In this case, EOF along the electric field lines is accompanied by flow in opposite directions. The velocity vector representation in the detail plots Figs. 4(b) and 4(d) visualize the different flow patterns and the occurrence of loops in the closed system.

All experimental EOF maps refer to closed systems. Hence, the finding of stationary EOF recirculation patterns [see Fig. 3(b)] is not unexpected. This is in contrast to flow driven by external pressure gradients. The two-dimensional CFD simulation predicts a vortex at position 1 [see Fig. 3(a) and compare Fig. 4(d)], whereas the NMR experiment did not show any such recirculation pattern [Fig. 2(d)].

Remarkably, ECD maps do also reveal vortices. This is demonstrated in Figs. 2(b) and 3(c). A condition for such recirculation phenomena appears to be the presence of EOF, since the vortices disappear if the matrix consists of PS. A comparison of ECD maps with and without EOF is given in Figs. 2(b) and 2(c).

There is a tendency that the electro-osmotic effect favors the occurrence of eddies both of the flow velocity and electric current density (Fig. 3). However, the positions of the areas where vortex phenomena occur do not coincide. In the absence of EOF, no complete vortex pattern was found at any position neither for flow [Fig. 2(d)] nor for electric current [Fig. 2(c)]. The same applies to simulations of the EOF velocity in open systems [Fig. 4(b)].

Flow eddies attached to obstacles are well-known even for extremely low Reynolds numbers. On the other hand, the fact that electric current vortices have been observed appears to be remarkable in view of the known property $\vec{\nabla} \times \vec{E} = 0$ for electrostatic field strengths. Both in the experiments and CFD simulations, no coinciding recirculation patterns could be identified for different transport quantities or different driving forces or different boundary conditions at the electrodes. This raises the question of similitude between the fluid velocity and electric field in

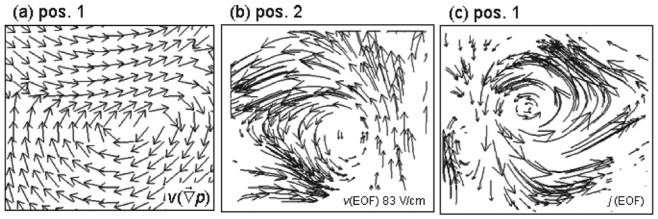

FIG. 3. Vortices of different transport quantities at positions 1 or 2 [see Fig. 1(b)]. (a) Two-dimensional CFD simulation of the flow velocity driven by an external pressure gradient at position 1 (area 0.8 mm × 0.8 mm). (b) Experimental EOF velocity at position 2 (area 1.2 mm × 1.2 mm) in streamline representation. (c) Experimental ECD in the presence of EOF at position 1 (area 1.2 mm × 1.2 mm) in streamline representation.

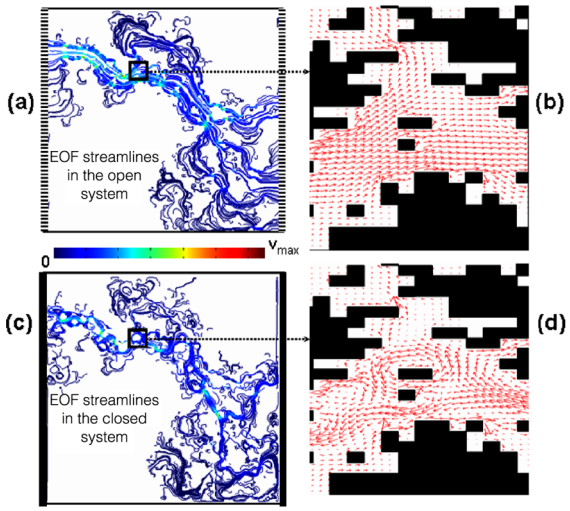

FIG. 4 (color online). Comparison of CFD simulations of EOF in open and closed two-dimensional random-site percolation clusters. The "percolating" cluster is shown in Fig. 1. (a) Streamlines in an open system with permeable electrodes on the left and right. Inflow and outflow from and to reservoirs is assumed to be unrestricted in this case. The matrix is not shown. The color (or gray shade) of the streamlines encodes the local velocity. (b) Enlarged velocity vector representation of the area marked in (a). The matrix is now rendered in black. (c) and (d) Same as (a) and (b), but now for a closed system excluding any inflow or outflow. The different flow patterns are obvious when considering the vector representations in (b) and (d).

EOF as discussed in Ref. [7]. All our EOF experiments refer to closed electrodes. That is, the Helmholtz-Smoluchowski equation which relates the flow velocity linearly with the electric potential gradient is not satisfied at those boundaries. This is considered to be the main reason why the similitude conditions of Ref. [7] do not apply.

The electrodynamic and hydrodynamic transport patterns in the presence and absence of electro-osmosis in complex systems reported here are important for applications in microsystem technology [25]. Microsystem devices often consist of complex channel networks implying features of the model objects of the present study. Based on a structure producing closed-loop flow, cyclic electro-osmotic pumps can be designed, for example. The intentional production of recirculation in such systems is essential for the function of microsystem mixers as discussed in Ref. [26]. Generally, the combined application of NMR microscopy techniques for the quantitative, noninvasive visualization of the total variety of hydrodynamics and electrodynamics in the same channel system is a promising design tool in microsystem technology. In this sense, the NMR methods used here are unique and superior to conventional fluid dynamics techniques such as particle image, ultrasound Doppler, or laser Doppler velocimetry [27,28].

[1] D. Li, *Electrokinetics in Microfluidics* (Elsevier, London, 2004).
[2] R. F. Probstein, *Physicochemical Hydrodynamics* (Wiley, New York, 1994).
[3] W. Zhu, S. J. Singer, Z. Zheng, and A. T. Conlisk, Phys. Rev. E **71**, 041501 (2005).
[4] S. Yao and J. G. Santiago, J. Colloid Interface Sci. **268**, 133 (2003).
[5] D. Wu, A. Chen, and C. S. Johnson, Jr., J. Magn. Reson., Ser. A **115**, 123 (1995).
[6] B. Manz, P. Stilbs, B. Jönsson, O. Söderman, and P. T. Callaghan, J. Phys. Chem. **99**, 11 297 (1995).
[7] E. B. Cummings, S. K. Griffiths, R. H. Nilson, and P. H. Paul, Anal. Chem. **72**, 2526 (2000).
[8] D. Stauffer and A. Aharony, *Introduction to Percolation Theory* (Taylor and Francis, London, 1992).
[9] A. Klemm, R. Kimmich, and M. Weber, Phys. Rev. E **63**, 041514 (2001).
[10] M. Weber and R. Kimmich, Phys. Rev. E **66**, 056301 (2002).
[11] R. Kimmich, *NMR Tomography, Diffusometry, Relaxometry* (Springer, Berlin, 1997).
[12] M. Weber and R. Kimmich, Phys. Rev. E **66**, 026306 (2002).
[13] D. Long, H. A. Stone, and A. Ajdari, J. Colloid Interface Sci. **212**, 338 (1999).
[14] Y. Manassen, E. Shalev, and G. Navon, J. Magn. Reson. **76**, 371 (1988).
[15] G. C. Scott, M. L. G. Joy, R. L. Armstrong, and R. M. Henkelman, J. Magn. Reson. **97**, 235 (1992).
[16] E. Kossel, B. Buhai, R. Kimmich in *NMR Imaging in Chemical Engineering*, edited by S. Stapf and S.-I. Han (Wiley-VCH, Weinheim, 2005), Chap. 2.9.
[17] D. C. Ghiglia and M. D. Pritt, *Two Dimensional Phase Unwrapping* (Wiley, New York, 1998).
[18] C. L. Rice and R. Whitehead, J. Phys. Chem. **69**, 4017 (1965).
[19] R. J. Hunter, *Foundations of Colloidal Science* (Oxford University Press, Oxford, 1987), Vol. 2, p. 786.
[20] J. D. Anderson, *Computational Fluid Dynamics* (McGraw-Hill, New York, 1995).
[21] C. Cuvelier, A. Segal, and A. van Steenhoven, *Finite Element Methods and Navier-Stokes Equations* (Reidel, Dordrecht, 1988).
[22] *FEMLAB User's Guide* (Comsol AB, Stockholm, 2004).
[23] A. Ajdari, Phys. Rev. E **53**, 4996 (1996).
[24] P. Bendel, M. Bernardo, J. H. Dunsmuir, and H. Thomann, Phys. Rev. E **67**, 046307 (2003).
[25] Y. Takamura, H. Onoda, H. Inokuchi, S. Adachi, A. Oki, and Y. Horiike, Electrophoresis **24**, 185 (2003).
[26] H. Chen, Y. T. Zhang, I. Mezic, C. D. Meinhart, and L. Petzold, *Proc. Microfluidics 2003* (ASME IMECE, New York, 2003).
[27] E. Guyon, J.-P. Hulin, L. Petit, and C. D. Mitescu, *Physical Hydrodynamics* (Oxford University Press, New York, 2001).
[28] D. Yan, N. T. Nguyen, C. Yang, and X. Huang, J. Chem. Phys. **124**, 021103 (2006).